

Composition and structure of the GaN{000 $\bar{1}$ }- (1×1) surface

M. M. Sung, J. Ahn, V. Bykov, and J. W. Rabalais*

Department of Chemistry, University of Houston, Houston, Texas 77204-5641

D. D. Koleske and A. E. Wickenden

Code 6861, Naval Research Laboratory, Washington, D.C. 20375-5347

(Received 5 June 1996)

The composition and structure of the *n*-type GaN{000 $\bar{1}$ }- (1×1) surface of samples grown on sapphire by organometallic vapor-phase epitaxy (OMVPE) has been determined through the use of time-of-flight scattering and recoiling spectrometry (TOF-SARS), three-dimensional classical ion trajectory simulations, low-energy electron diffraction (LEED), and thermal decomposition mass spectrometry (MS). Elastic recoil detection was used to determine the bulk hydrogen concentration. TOF-SARS spectra of scattered and recoiled ions plus fast neutrals were collected as a function of crystal azimuthal rotation angle δ and beam incident angle α using 4 keV Ne⁺ or Ar⁺ primary ions in order to determine the surface termination layer, presence and location of impurities, and possible reconstruction or relaxation. LEED, TOF-SARS, and MS were monitored as a function sample temperature up to the point of decomposition. The totality of these data leads to the conclusions that the (1×1) surface is neither reconstructed nor relaxed, that it is terminated in a N layer, that Ga comprises the second layer, that there are two domains rotated by 60° from each other, and that there are steps on the surface. Hydrogen atoms are bound to the outerlayer N atoms and protrude outward from the surface with a coverage of $\sim\frac{3}{4}$ monolayer, facilitating autocompensation of the (1×1) structure. The bulk hydrogen concentration is $\sim 4\times 10^{19}$ atoms/cm³. Evolution of gases commences at ~ 850 °C with the observed evolution of N₂, NH₂, and H₂. These results are discussed in terms of reconstruction phenomena, autocompensation, film/substrate polarity matching, and the role of hydrogen in stabilizing the growth of GaN. [S0163-1829(96)06844-0]

I. INTRODUCTION

The group-III nitrides,¹⁻³ specifically GaN, have a large cohesive energy compared to group-III phosphides and arsenides. This arises from the high electronegativity of nitrogen and the partial ionic character of the Ga-N bonds.⁴ The increased cohesive bond energy of the nitrides results in the wide-band-gap emission which is observed in GaN-based diodes^{5,6} and lasers.⁷ The nitrides are also chemically stable, making them attractive for high-power and high-temperature device applications.¹⁻³ Although different growth techniques are used, thin films of GaN are primarily grown using either molecular-beam epitaxy (MBE) or organometallic vapor-phase epitaxy (OMVPE). GaN films grown with either technique can have similar electrical properties,⁸ however, GaN films grown by OMVPE typically have higher electron mobility and faster growth rates.

Two major differences exist between the MBE and OMVPE growth techniques: (1) the growth temperature and (2) the amount of hydrogen present during growth. In MBE, the GaN growth temperature ranges from 600–800 °C and no (or very little) hydrogen is present during the growth.³ In OMVPE, the GaN growth temperature ranges from 1000–1100 °C and there is a substantial amount of hydrogen present in the NH₃, Ga-alkyl precursors, and in the carrier gas (when H₂ is used³). The nature of hydrogen in GaN as well as its role in the growth of GaN are incompletely understood. A recent theoretical study⁹ has shown that hydrogen in GaN behaves very differently compared to the well-established behavior in more traditional semiconductors, i.e., it has a high diffusivity and a strong preference for sites with

high charge density near the electronegative N atoms. Concerning its effect on growth, it is believed that high growth temperatures are needed in the OMVPE process to activate the NH₃ for growth and perhaps to desorb hydrogen from the surface.¹⁰ Also, in OMVPE growth, hydrogen is known to complex with Mg in *p*-type doping of GaN, rendering the Mg electrically inactive.^{11,12} Only through low-energy electron-beam irradiation¹¹ or high-temperature annealing¹² can the H:Mg complex be dissociated to activate the Mg. Theoretical calculations also suggest that the H:Mg complex incorporation into the GaN lattice has a lower activation energy than for uncomplexed Mg.¹³ This is a possible explanation as to why relatively large amounts of hydrogen are found in *p*-type GaN while little is present in *n*-type films.¹³ In highly resistive (i.e., $>10^{10}$ Ω/cm²) GaN there can be substantial amounts of hydrogen (as high as 10^{18} cm⁻³) as well as other impurities (O and C) in the films,¹⁴ which suggest that these impurities are electrically compensating or inactive. Therefore, hydrogen may chemically stabilize potential dopant, defect, and surface sites in the lattice during growth.

Since no lattice matched substrate currently exists for GaN growth,¹⁵ sapphire and 6H-SiC are commonly used.³ The GaN films grown on these substrates relieve strain by creating misfit dislocations, hence these films have little strain, but large defect densities (10^8 – 10^{10} cm⁻²). GaN films have been shown to have slightly different lattice constants depending on the growth substrate.¹⁶ This slight difference in the lattice constant can be observed in the photoluminescence peak shifts. It is not clear if hydrogen incorporation into the lattice can reduce strain or if hydrogen migrates to

the misfit dislocations. Films can be grown that are highly resistive, suggesting that the defects are either electron traps or compensating centers.

The nature of the surface termination layer and the structure of the GaN{000 $\bar{1}$ }-(1×1) surface has not been determined experimentally. Understanding the chemical bonding and structure of the GaN surface provides a starting point for determining the mechanistic details from precursor decomposition to incorporation into the GaN film. In addition, the success of GaN electronic devices is dependent on the atomic level control of the elemental compositions. This is especially important at the interfaces where compositional changes are made, e.g., in quantum well or heterojunction structures. One simple question is the extent of GaN{000 $\bar{1}$ } surface reconstructions or relaxations and the possible surface structures. For example, GaAs{111} and GaP{111}, which would be the zinc-blende phase analogs to the wurtzite GaN{000 $\bar{1}$ } surface, are known¹⁷ to form (2×2) reconstructions with the cation terminated {111}-(2×2) surface having a Ga vacancy surrounded by a cyclic anion structure and the anion terminated ($\bar{1}\bar{1}\bar{1}$)-(2×2) surface having a trimer structure. These reconstructions reduce the number of dangling bonds, thereby lowering the surface free energy and producing a surface which is autocompensated. Autocompensation is the transfer of electrons from the more electropositive elements (group III) to the more electronegative elements (group V) in order to produce a surface in which all anion dangling bonds are filled and all cation dangling bonds are empty; such a surface exhibits semiconducting behavior. However, because of the large Ga-N bond energy, the resistance to relaxation or reconstruction of the {000 $\bar{1}$ } surface may be high. This has recently been confirmed by theoretical calculations which predict¹⁸ that the GaN{001} surface is unreconstructed and should have a (1×1) surface pattern. Such an unreconstructed (1×1) surface is not autocompensated; passivation of such a surface can be achieved by bonding of the N dangling bonds to foreign atoms.

The techniques of low-energy electron diffraction (LEED),^{19,20} reflection high energy electron diffraction (RHEED),^{21,22} x-ray and ultraviolet photoelectron spectroscopy (XPS and UPS),^{19,20,23-27} Auger electron spectroscopy (AES),^{19,20} and electron-energy-loss spectroscopy (ELS)^{19,20} have been used to study GaN surfaces. LEED and RHEED results have shown^{19,20} that the well-ordered surfaces exhibit a sharp (1×1) pattern; some of the RHEED studies²² have found a streaky (2×2) pattern. These latter studies were performed under a Ga-rich environment such that there was an excess of Ga at the surface; this may explain the observed RHEED pattern. The XPS and AES studies^{19,20,23-27} have characterized the core-level binding energies and fine structure of the Ga LMM transition. It has been suggested²⁰ that the clean {000 $\bar{1}$ }-(1×1) surface is N terminated, based on AES measurements. A recent *ab initio* total-energy calculation²⁸ of GaN growth on SiC has shown that polarity matching at the film/substrate interface plays a fundamental role in determining the lower-energy structures and, hence the termination layer of the film. Such polarity matching will only be important if the stacking sequence of the films is preserved.

In this paper the surface and bulk composition, termination layer, and structure of a GaN{000 $\bar{1}$ }-(1×1) film grown

on a sapphire wafer are investigated. The designations {000 $\bar{1}$ } and {0001} are used for the N and Ga terminated surfaces, respectively. The techniques of time-of-flight scattering and recoiling spectrometry (TOF-SARS), classical ion trajectory simulations, LEED, and thermal decomposition mass spectrometry (MS) were used in the surface analysis. The bulk hydrogen concentration was determined by elastic recoil detection (ERD). The combination of the techniques allows characterization of the elemental composition in the outermost two atomic layers, the elements that comprise the surface termination layer, the surface symmetry, and possible reconstructions or relaxations. In addition, TOF-SARS has high sensitivity to surface hydrogen and allows one to probe the involvement of hydrogen in the surface structure.

II. EXPERIMENTAL METHODS

A. GaN sample

1. GaN film growth on sapphire

GaN was grown on the *c* plane {000 $\bar{1}$ } of polished sapphire using the NRL facilities. This consisted of a vertical, inductively heated, water-cooled quartz OMVPE reactor at reduced pressure (57 torr) using H₂ as the carrier gas.²⁹ After annealing in H₂, the wafer was cooled to ~ 450 °C and a 200-Å nucleation layer of AlN was grown using 1.5 μ mole/min triethylaluminum and a 2.5-standard liters/min (slm) flow of NH₃. The substrate was then heated to the growth temperature of 1040 °C and GaN was grown using 53 mmole/min or trimethylgallium under an NH₃ flow of 2.25 slm. The films were uniformly doped using 8 ppm Si₂H₆ in H₂ at a flow rate of 0.36 standard cubic centimeters/min (scm).³⁰ After growth of a 2.7- μ m-thick GaN film, the substrate was cooled in the NH₃ flow at a rate of 50 °C per minute. The *n*-type films investigated in this study had an electron concentration of 1.2×10^{17} cm⁻³ and a mobility of 325 cm²/V s. The x-ray rocking curve full width at half maximum was 350 arc sec; this is a measure of the mosaic structure of the GaN thin film.

2. Cleaning GaN in vacuum

The $\sim 1\times 1$ -cm² samples were cleaned in the UHV chamber (base pressure $<5\times 10^{-10}$) used for TOF-SARS at the University of Houston. The samples were mounted on the TOF-SARS sample holder with the sapphire substrate in contact with a Ta plate and held together by small Ta strips over the sample edges. Annealing was achieved by radiative heating and electron bombardment from a tungsten filament mounted behind the Ta plate. Temperatures were measured by means of pyrometer and a thermocouple which was attached to the sample; the pyrometer readings were calibrated by the thermocouple. The absolute temperature measurements have a maximum uncertainty of ± 20 °C. The clean surface was prepared by cycles of sputtering (1 keV N₂⁺ ions, 0.5 μ A/cm², 10 min) and annealing (10 min) using a dynamic N₂ backfill. This procedure has been shown to produce a clean stoichiometric surface.³¹ A faint (1×1) LEED pattern became discernible at ~ 815 °C and evolved into a sharp hexagonal (1×1) pattern at ~ 920 °C. Upon continued heating to 1000 °C, a diffuse background and satellite spots around the hexagonal spots were observed, indicating pos-

sible surface faceting. Sample cleanliness was established by the absence of carbon and oxygen recoil peaks in the TOF-SARS spectra and the presence of a sharp (1×1) LEED pattern. The TOF-SARS spectra always showed the presence of H recoils when the sharp (1×1) pattern was observed. Three different GaN samples, which were all grown and cleaned as described above, were used for the TOF-SARS measurements. All three samples exhibited similar behavior and yielded similar results.

B. Analysis techniques

LEED patterns were obtained with Princeton Research Instruments, Inc. reverse view optics. Mass spectra (MS) were acquired with a Leybold-Inficon, Inc. quadrupole residual gas analyzer. The technique of ERD with MeV ions, which is capable of both bulk and near surface analysis, was used to determine the hydrogen concentration in GaN.

The TOF-SARS technique was used for surface elemental composition analysis and atomic structure characterization. Details of the TOF-SARS technique have been described elsewhere.³² Briefly, a pulsed noble gas ion beam irradiates the sample surface in a UHV chamber and the scattered and recoiled ions plus fast neutrals are measured by TOF techniques. The primary 4-keV beam employed herein was Ne^+ for scattering from Ga atoms and Ar^+ for recoiling of H, N, and Ga atoms. The ion pulse width was ~ 50 ns and the pulse repetition rate was 30 kHz, resulting in a flux of $\sim 2 \times 10^5$ ions/pulse. The angular notation is defined as follows: α =beam incident angle to the surface, δ =crystal azimuthal angle, θ =scattering angle, ϕ =recoiling angle, and β =scattering or recoiling exit angle from the surface. A schematic drawing of the unreconstructed $\text{GaN}\{000\bar{1}\}$ surface is shown in Fig. 1; the $\langle 1000 \rangle$ azimuth is defined as $\delta=0^\circ$.

C. Classical ion trajectory simulations

Classical ion trajectory simulations were carried out by means of the three-dimensional scattering and recoiling imaging code (SARIC) developed at UH. SARIC is based on the binary collision approximation, uses the ZBL universal potential to describe the interactions between atoms, and includes both out-of-plane and multiple scattering. Details of the simulation have been published elsewhere.³³

III. RESULTS

A. Identification of the first-layer species and hydrogen analysis

1. Termination layer

Elemental analysis was obtained by matching the observed TOF peaks to those predicted by the binary collision approximation.³⁴ The first-layer elemental species was determined by using grazing incidence ($\alpha=6^\circ$) TOF-SARS at random azimuthal angles and a scattering-recoiling angle of $\theta=\phi=40^\circ$. Using random azimuthal angles and a low incident angle avoids the anisotropic effects of scattering along the principal low-index azimuths and provides scattering intensities which are from the first-atomic layer and exposed atoms in the second-atomic layer.

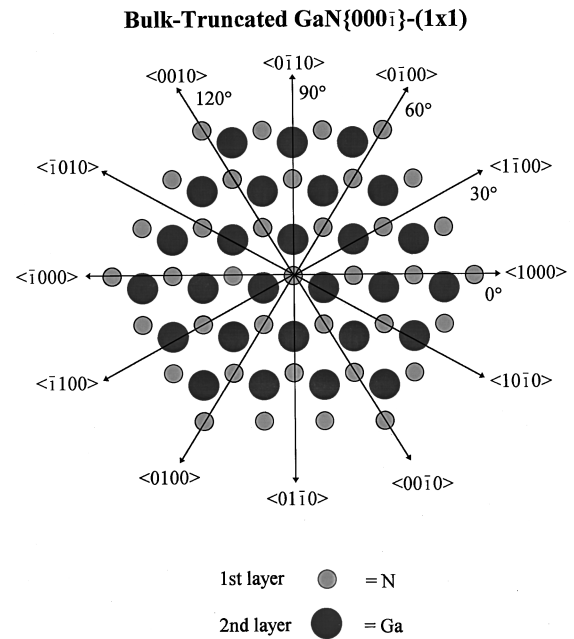


FIG. 1. Plan view of the ideal bulk-terminated $\text{GaN}\{000\bar{1}\}$ surface illustrating the azimuthal angle δ assignments. Another domain is obtained by 180° rotation of this surface about the surface normal. Open circles, first-layer N atoms; large solid circles, second-layer Ga atoms. The sizes of the circles are proportional to the atomic radii.

A typical TOF spectrum from a $\text{GaN}\{000\bar{1}\}$ -(1×1) surface taken along a random azimuthal direction (not aligned along a high symmetry azimuth) with a grazing incident angle α is shown in Fig. 2. Under these conditions the observed scattering features are almost exclusively from the first- and second-atomic layers. The spectrum exhibits peaks due to scattering of Ar from Ga atoms and recoiling of H, N, and Ga atoms. The TOF's and corresponding energies of these scattered and recoiled atoms are consistent with the binary collision approximation. The scattering angle used

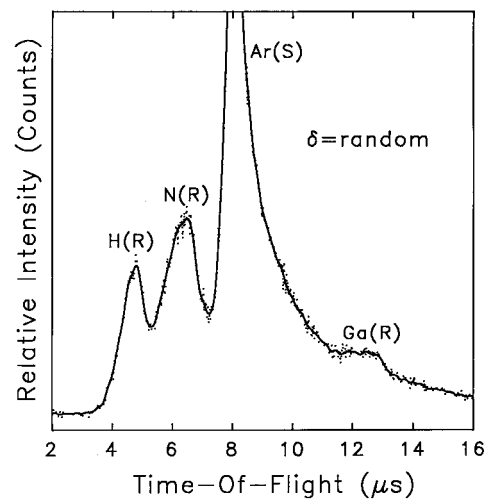


FIG. 2. TOF-SARS spectrum of 4 keV Ar^+ scattering from a $\text{GaN}\{000\bar{1}\}$ -(1×1) surface with the ion beam aligned along a random azimuthal direction. Incident angle $\alpha=6^\circ$; scattering angle $\theta=40^\circ$.

TABLE I. Calculated cross sections (σ) for 4-keV Ar⁺ scattering from Ga atoms and recoiling of H, N, and Ga atoms, relative atomic concentrations from experimental intensities along random azimuths, and ASEA values.

Scattering (<i>S</i>) and recoiling (<i>R</i>) cross sections (σ) [\AA^2]			
$\sigma_{\text{Ga}}(S)$	$\sigma_{\text{H}}(R)$	$\sigma_{\text{N}}(R)$	$\sigma_{\text{Ga}}(R)$
0.21	0.13	0.071	0.099
Relative surface atomic concentrations			
[N]=1	[H]=0.71	[Ga]=0.091	
Experimental ^a ASEA values along the 0° <100> and 30° <110> azimuths			
$(I_{30^\circ}/I_{0^\circ})_{\text{N}}=1.0$	$(I_{30^\circ}/I_{0^\circ})_{\text{H}}=1.1$	$(I_{30^\circ}/I_{0^\circ})_{\text{Ga}}=0.59$	
Simulated ^a ASEA values along the 0° <100> and 30° <110> azimuths			
$(I_{30^\circ}/I_{0^\circ})_{\text{N}}=1.0$	$(I_{30^\circ}/I_{0^\circ})_{\text{H}}=0.8$	$(I_{30^\circ}/I_{0^\circ})_{\text{Ga}}=0.17$	

^aRatios of recoiling peaks for N and H and scattering peaks for Ga were used in calculating both the experimental and simulated ASEA values.

($\theta = 40^\circ$) is above the critical angle for Ar single scattering from N atoms ($\theta_c = 20.5^\circ$). This results in a negligible contribution of the N atoms to the scattering peak intensity in the region of 8–9 μs since Ar double scattering from two N atoms (assuming two scattering angles of $\theta = 20^\circ$ each) would have a TOF of $\sim 17 \mu\text{s}$. The relative elemental concentrations in the surface layers were obtained from spectra similar to that of Fig. 2, which were collected at five different random azimuthal angles. The relative H, N, and Ga recoil intensities were obtained from the average of these five spectra, from which concentrations were calculated after background subtraction and correction for the different recoiling cross sections. The cross sections were calculated in the binary collision approximation using the Moliere approximation to the potential function. The calculated cross sections and relative atomic concentrations are listed in Table I. The Ga recoiling peak rather than the scattering peak was used for the concentration determination because comparison between only scattering or only recoiling peaks provides more accuracy than comparison between both scattering and recoiling peaks. Relative concentrations obtained in this manner have an uncertainty on the order of 30%, primarily due to shadowing and blocking effects which are not corrected along the random azimuths.

The high ratio $[\text{N}]/[\text{Ga}] = 6.3$ from Table I provides compelling evidence that the surface is terminated in a layer of N atoms and that the Ga atoms occupy the second layer. The intense H recoil peak was present under all conditions that gave rise to the clear (1 \times 1) LEED pattern. The comparable intensities of the H and N recoil peaks indicates that the concentrations of these two elements on the (1 \times 1) surface are also comparable.

3. Hydrogen analysis

ERD analysis was performed with a 7.9-MeV C⁴⁺ beam at a grazing incident angle of 13° and exit angle of 15° using

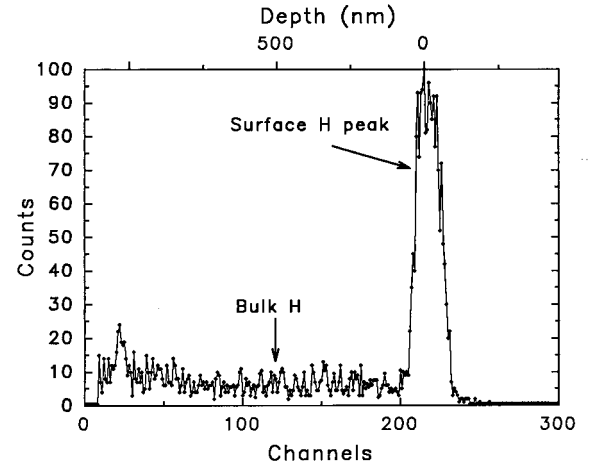


FIG. 3. ERD spectrum of H atoms from GaN{0001}-(1 \times 1) using 7.8 MeV C⁴⁺ ions at a grazing incidence angle of 13° and exit angle of 15°.

a GaN sample on which no cleaning attempt was made. A surface hydrogen recoil peak as well as a continuous background due to subsurface hydrogen were observed as shown in Fig. 3. The absolute hydrogen concentrations were obtained by comparison to a standard of amorphous silicon which was implanted with 1×10^{17} H atoms/cm². The observed “surface” hydrogen peak corresponds to an areal density of 1.5×10^{16} H atoms/cm² and the continuous background corresponds to a “bulk” density of 4.0×10^{19} H atoms/cm³. For an ideal GaN crystal, the N or Ga atom surface density is 1.1×10^{15} atoms/cm² and the bulk density is 4.4×10^{22} atoms/cm³. The observed “bulk” H concentration is low while the surface concentration is abnormally high. This apparently abnormally high surface hydrogen concentration obtained from ERD results from the emergence of the high-energy elastically recoiled H atoms from a depth of some 5–10 atomic layers. The bulk sampling is down to ~ 1000 nm.

B. Determination of the bulk crystallographic directions

1. Composition from azimuth-specific elemental accessibilities (CASEA) method

CASEA (Ref. 35) provides information on the relative elemental accessibilities along selected low index azimuths. These values are useful in confirming the results from the elemental analysis and the crystal structure. The scattering or recoiling peak intensities are measured under conditions of low incident angle α , low exit angle β , and alignment of the beam along selected low-index azimuths δ . Due to the shadowing and blocking effects, measurements with these incident and exit angles provide scattering and recoiling intensities that come from only those layers of atoms that are directly exposed to the vacuum. Since only the first- and second-layer atoms, or atoms exposed in missing-row troughs, are accessible to the beam under these conditions, azimuth-specific elemental accessibilities (ASEA) along the azimuths are obtained. These ASEA results are used in relating the orientation of the surface symmetry elements, i.e., the features of the LEED pattern, as follows. For a given ele-

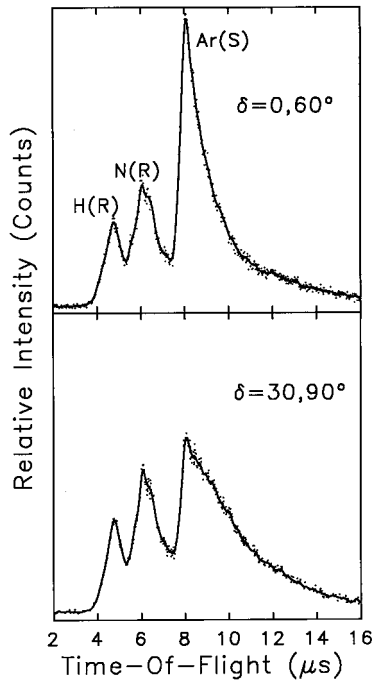


FIG. 4. TOF-SARS spectra of 4-keV Ar^+ scattering from $\text{GaN}\{000\bar{1}\}_-(1\times 1)$ with the ion beam directed along the $\langle 1000 \rangle$ ($\delta = 0^\circ$) and $\langle 1100 \rangle$ ($\delta = 30^\circ$) directions. Incident angle $\alpha = 12^\circ$; scattering angle $\theta = 40^\circ$.

ment (i), the ASEA is the ratio of scattering or recoiling intensities (I) from the element along two different azimuthal directions (χ & δ) of the crystal. Using a simple shadow cone approximation, the ASEA is equal to the ratio of the number of atoms $[N_\chi/N_\delta]_i$ exposed to the beam in the surface unit cell of the surface phase for the two azimuths, i.e.,

$$(I_\chi/I_\delta)_i = \text{ASEA}_i = [N_\chi/N_\delta]_i.$$

This ratio is independent of scattering and recoiling cross section corrections.

It will be sufficient to observe the ASEA values along the 0° and 30° azimuths because there are two domains on the surface (as will be shown later). Along the 0° azimuth, the second-layer atoms are partially shadowed by the first-layer atoms because the lateral and vertical spacings between them are only 0.9 and 0.63 Å, respectively, and the radii of the shadow cones are of the order of 1 Å. Along the 30° and 90° azimuths, it is possible for the first-layer atoms to totally shadow second-layer atoms, making them inaccessible for scattering. Example spectra used in obtaining the ASEA values are shown in Fig. 4 and the results are listed in Table I. Although the degree of shadowing is different for projectiles approaching along the 30° or 90° directions due to the proximity of the first- and second-layer atoms, the Ar^+ scattering intensities from the Ga atoms along the two directions are the same; this signifies the presence of two domains on the surface. These results show that the H and N atom ASEA values are independent of the azimuthal orientation. This is possible only if the outermost layer of the crystal is composed of N atoms. The H atoms are most likely bound to these N atoms, constituting an overlayer. Shadowing or blocking of the N atoms by the overlayer of H atoms is

negligible because the heavier particles penetrate the H atom shadowing or blocking cones with negligible deflection. The Ga accessibility is extremely sensitive to azimuthal direction; specifically, it is greatly reduced along the 30° direction, confirming that Ga is a second-layer atom and that the 30° direction corresponds to the $\langle 1100 \rangle$ azimuth (see Fig. 1).

The difference in the ASEA values along the principal azimuths can be confirmed by ion trajectory simulations using the structure of Fig. 1. Simulations were performed for ions approaching along the 0° , 30° , and 90° directions. The 30° and 90° directions present different arrangements of the underlying atoms with respect to the first-layer atoms. Since there are two domains on the surface (as will be shown later), the simulated ASEA values were averaged along the 30° and 90° directions for comparison to the experimental value measured at 30° . The results, listed in Table I, are in qualitative agreement with the experimental ASEA values, i.e., the ASEA values for H and N are azimuthally insensitive while the ASEA value of Ga is azimuthally sensitive, exhibiting a minimum along the $\delta = 30^\circ$ direction. The experimental ASEA value for Ga is less sensitive to the azimuthal angles than the simulated value. This indicates that the surface is highly stepped because the Ga accessibility is relatively insensitive to the azimuthal direction at the step edges. Quantitative agreement between experiment and simulated ASEA values is seldom obtained for highly stepped surfaces (see Sec. III B 2) because the simulation uses a perfect crystal structure and collimated in beam whereas the experiment is performed on an imperfect crystal using an ion beam with finite divergence.

2. Incident angle α scans

Information on the subsurface structure along planes perpendicular to the surface can be obtained³⁶ by measuring scattering intensity from Ga (I_{Ga}) as a function of the incident angle α along the azimuthal directions $\delta = 0^\circ$ $\langle 1000 \rangle$ and 30° $\langle 1100 \rangle$. At grazing α , all atoms lie within the shadow cones of their preceding neighbors.³⁶ As α is increased, subsurface layer atoms move out of the shadow cones of the first-layer atoms. When the impact parameter required for scattering into θ becomes accessible, a sharp increase in I_{Ga} is observed due to focusing of ion trajectories at the edges of the shadow cones. Examples of such α scans are shown in Fig. 5. The high scattering angle of $\theta = 120^\circ$ is above the critical scattering angle for Ne^+/N collisions ($\theta_c = 44^\circ$); as a result, the scattering features are dominated by quasisingle scattering collisions of Ne^+/Ga . The α scans along the 30° and 90° (not shown) azimuths exhibited identical features. This is indicative of the existence of two different surface domains that are rotated by 60° ; if there would be only one domain, different features of the α scans would be expected.

The large peak at low α results from Ne scattering from second layer Ga. The nonzero value of I_{Ga} at $\alpha = 0^\circ$ and the sharp increase in I_{Ga} at very low α also indicate that the surface has a highly stepped structure; a flat surface with few steps would have no observable I_{Ga} at $\alpha = 0^\circ$ and the first peak would be at higher α , i.e., $\sim 20^\circ$ – 25° rather than the observed position of $\sim 10^\circ$.

The smaller peaks observed in Fig. 5 at higher α are due to scattering from subsurface Ga atoms. Ion trajectory simulations are shown on the right side of Fig. 5 along planes that

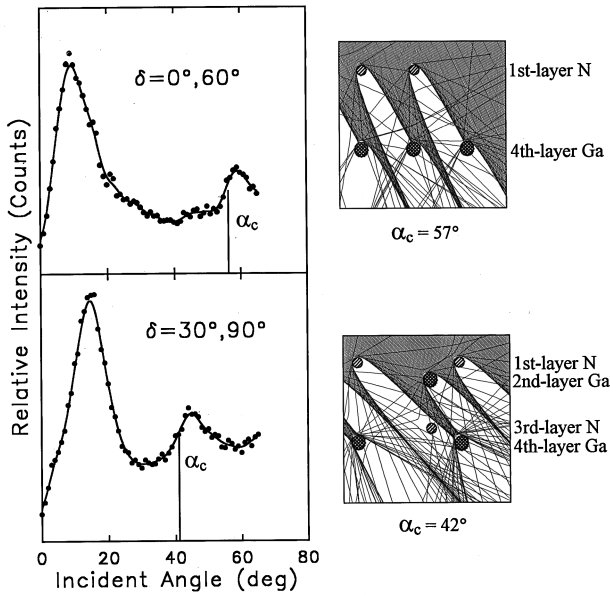


FIG. 5. Incident angle α scans of 4 keV Ne^+ scattering intensity from Ga along the $\langle 1000 \rangle$ ($\delta=0^\circ$) and $\langle 1\bar{1}00 \rangle$ ($\delta=30^\circ$) azimuths of the $\text{GaN}\{000\bar{1}\}$ - (1×1) surface. The scattering angle was $\theta=120^\circ$. Ion trajectory simulations are shown on the right-hand side of the scans along planes which are perpendicular to the $\{000\bar{1}\}$ surface and contain the 0° and 30° azimuths. Bulk interatomic spacings were used for the simulations.

are perpendicular to the $\{000\bar{1}\}$ surface and contain the 0° and 30° azimuths. Along $\delta=0^\circ$ the N atoms in the first bilayer are aligned with Ga atoms in the second bilayer. Planar focusing from the first-bilayer N atoms onto the second-bilayer Ga atoms is possible at a critical incident angle of $\alpha_c=57^\circ$; the experimental feature in Fig. 5 commences at $\sim 55^\circ$ and peaks at $\sim 59^\circ$. Along $\delta=30^\circ$ or 90° the N and Ga atoms in the first and second bilayers are also aligned in the same plane; however, the interatomic spacings along this azimuth are different. Planar focusing from the first-bilayer N atoms onto the second-bilayer Ga atoms is possible at a critical incident angle of $\alpha_c=42^\circ$; the experimental feature in Fig. 5 commences at $\sim 37^\circ$ and peaks at $\sim 44^\circ$. Also note that along this azimuth the trajectories are double focused by the first-bilayer N and Ga atoms onto the second-bilayer Ga atoms, resulting in the higher relative intensity of the subsurface peak along $\delta=30^\circ$ compared to $\delta=0^\circ$. The results of these α scans support the structures proposed in the previous sections and the correspondence of the 30° direction with the $\langle 1\bar{1}00 \rangle$ azimuth. As shown in Fig. 5, the simulated α_c values (using the bulk interatomic spacings) agree well with the rising slopes of the experimental peaks. This indicates that any change in first- and second-interlayer spacing due to relaxation is within the accuracy of the measurement, i.e., the experimental uncertainty is $\pm 2^\circ$, which corresponds to an uncertainty in the interlayer spacing of $\pm 0.2 \text{ \AA}$.

C. Surface periodicities of the H, N, and Ga atoms

1. Azimuthal angle δ scans

The surface periodicities³⁷ of the H, N, and Ga atoms were determined by monitoring I_{Ga} for Ne scattering from

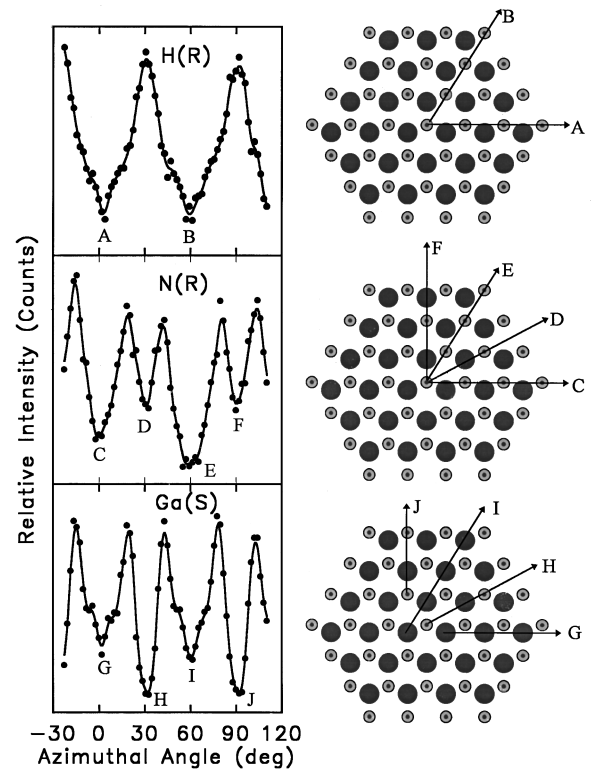


FIG. 6. Experimental azimuthal angle δ scans of Ne^+ scattering from Ga (I_{Ga}) along with H (I_{H}) and N (I_{N}) recoiling from Ar^+ on the $\text{GaN}\{000\bar{1}\}$ - (1×1) surface. The projectile was 4 keV Ne^+ and Ar^+ and the conditions were $\alpha=20^\circ$, $\theta=30^\circ$ for H, $\alpha=10^\circ$, $\theta=40^\circ$ for N, and $\alpha=12^\circ$, $\theta=90^\circ$ for Ga. The solid lines are smooth curves drawn through the data points to guide the eye. The small black dots on the N atoms represent H atoms at a full monolayer coverage.

Ga atoms and I_{H} and I_{N} for Ar recoiling of H and N atoms as a function of crystal azimuthal angle δ . TOF spectra similar to those of Figs. 2 and 4 were obtained and the intensities of the various peaks were plotted as a function of δ , resulting in the plots of Fig. 6. Maxima and minima are observed as a function of δ . The minima are coincident with low-index azimuths where the surface atoms are inside of the shadowing or blocking cones cast by their aligned, closely spaced nearest neighbor, resulting in low intensities. As δ is scanned, the atoms move out of the shadow cones along the intermediate δ directions where the interatomic spacings between the atoms are long, resulting in an increase in intensity. The widths of the minima are related to the interatomic spacings along that particular direction. Wide, deep minima are expected from short interatomic spacings because of the larger degree of rotation about δ required for atoms to emerge from neighboring shadows. Schematic diagrams of the GaN surface illustrating the scattering and blocking directions are presented along with the δ scans of Fig. 6. The geometrical parameters for these scans were chosen in order to provide maximum sensitivity to the structural features, different atomic masses, and different interatomic spacings along various azimuths.

The I_{N} δ scan (Fig. 6) was performed in the shadowing mode, i.e., a grazing incident angle of $\alpha=10^\circ$ was used. The data exhibit minima every 30° , with the minima labeled 0°

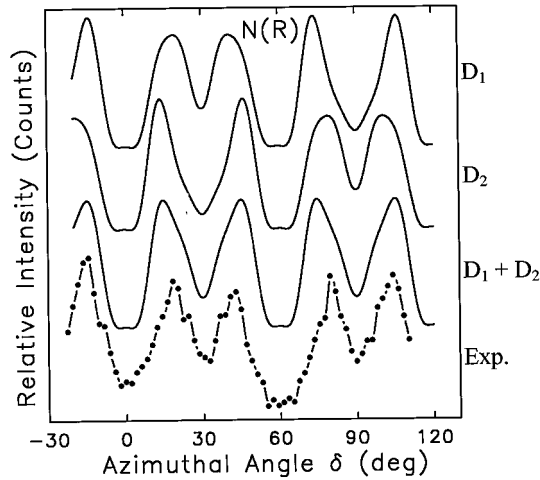


FIG. 7. Trajectory simulations of the azimuthal angle δ scan for N atoms recoiling from Ar^+ projectiles on a $\text{GaN}\{0001\}-(1\times 1)$ surface using the same conditions as listed in Fig. 6. Two different domains were used in the simulations. D_1 represents the single domain shown in Fig. 1, D_2 represents a single domain obtained by 180° rotation of the D_1 domain about its surface normal, and ($D_1 + D_2$) represents a combination of the single domain results using equivalent contributions from each domain. Exp. is the experimental data from Fig. 6 with smooth curves drawn through the data points to guide the eye.

and 60° being deeper than those at 30° and 90° . The 0° and 60° directions correspond to the $\langle 1000 \rangle$ and $\langle 0100 \rangle$ azimuths, respectively, where the N-N interatomic spacings are shortest and shadowing of first-layer N atoms by neighboring first-layer N atoms is most efficient. The 30° and 90° minima correspond to the $\langle 1100 \rangle$ and $\langle 0110 \rangle$ azimuths, respectively, where the N-N interatomic spacings are longer and shadowing is less efficient. As noted earlier, shorter interatomic spacings result in deeper and wider minima due to the larger azimuthal rotations required for atoms to move out of the shadow cones of their aligned nearest neighbors.

The I_{Ga} δ scan (Fig. 6) was also performed in the shadowing mode with an incident angle of $\alpha=12^\circ$. The data also exhibit minima every 30° , but in contrast to the I_{N} minima, the minima labeled 30° and 90° are deeper than those at 0° and 60° . Shadowing and blocking of second-layer Ga by first-layer N is most efficient along the 30° and 90° directions due to the aligned overlayer N atoms. Along the 0° and 60° directions, the overlayer N atoms are not aligned with the Ga atoms, resulting in less severe shadowing and blocking. As noted above, the degree of shadowing and blocking along the 30° and 90° azimuths is not identical due to the relationship of the first- and second-layer atoms. The minima observed at these two angles have identical widths and depths, suggesting that the surface exists in two different domains; if there would be only one domain, different widths and depths for these minima would be expected.

The I_{H} δ scan (Fig. 6) was performed in the blocking mode, i.e., a small exit angle $\beta=10^\circ$ was used. The data exhibit 60° periodicity with deep minima along the 0° and 60° directions, unlike the other two scans. The H atoms are too light to cause significant shadowing of the incoming Ar projectiles. However, recoiled H atoms can be blocked by first-layer neighboring N atoms. The radii of the shadowing

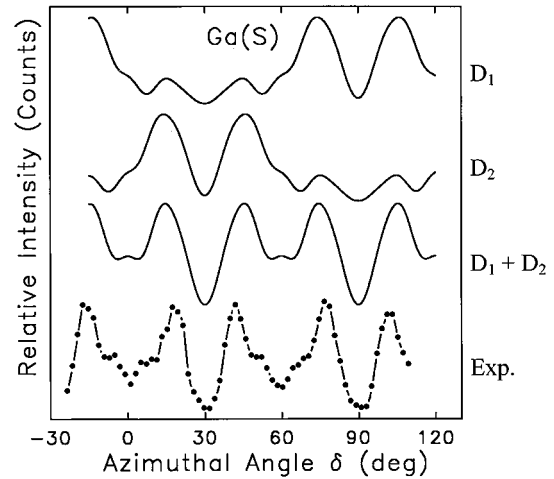


FIG. 8. Same as Fig. 7 for Ar^+ projectiles scattering from Ga atoms. Exp. is the experimental data from Fig. 6 with smooth curves drawn through the data points to guide the eye.

and blocking cones for H atom collisions with N and Ga atoms is only $<0.3 \text{ \AA}$ compared to $>1 \text{ \AA}$ for Ne^+ and Ar^+ collisions with N and Ga atoms.³⁸ By using a small exit angle β , recoiled H atoms can be blocked by nearest-neighbor N atoms. The observed periodicity arises if the H atoms are bound to the overlayer N atoms and protruding outward from the surface plane. The short H-N interatomic spacings along 0° and 60° result in overlayer recoiled H atoms being blocked by their first-layer N neighbors. Along the 30° and 90° directions, the H-N interatomic spacings are longer and the recoiling H trajectories are outside of the neighboring N atom blocking cones.

2. Simulations of the azimuthal scans of the N-terminated $\text{GaN}\{000\bar{1}\}-(1\times 1)$ surface

Trajectory simulations of the I_{N} azimuthal scan are shown in Fig. 7. The simulations were carried out for two different domains and for a combination of these two domains. When only a single domain is used, the azimuthal scans are not symmetrical about the 0° or 60° directions due to interactions of trajectories with the atoms of the second layer, which is shifted with respect to the first layer. Combining the two domains results in a symmetrical δ scan that is a good reproduction of the experimental scan. This is direct evidence for the presence of two domains with approximately equal abundance.

Trajectory simulations of the I_{Ga} azimuthal scan are shown in Fig. 8. The asymmetrical features of the single domain calculations are obvious. Combining the results from the two domains provides a symmetrical δ scan, which is in good agreement with the experimental δ scan.

Trajectory simulations of the I_{H} azimuthal scan are shown in Fig. 9 for a H atom coverage of $\frac{3}{4}$ of a monolayer arranged according to the model of Fig. 10. The reason for using a $\frac{3}{4}$ monolayer model is based on autocompensation predictions as will be discussed in Sec. IV B. The asymmetrical features of the single domain calculations are obvious, which shows that the H recoiling trajectories are sensitive to both first-layer N and second-layer Ga atoms. This indicates that the H

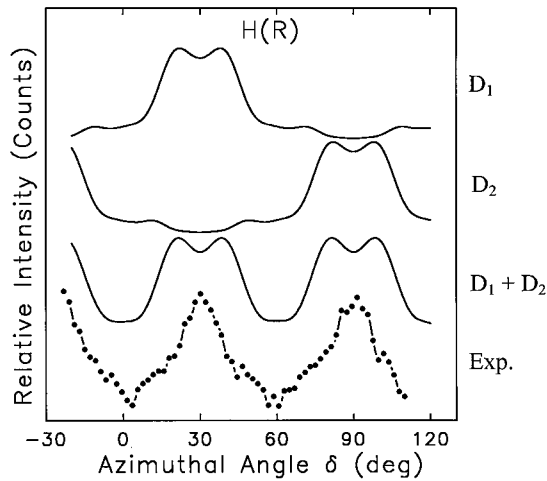


FIG. 9. Same as Fig. 7 for atoms recoiling from Ar^+ projectiles. Exp. is the experimental data from Fig. 6 with smooth curves drawn through the data points to guide the eye. The model for the H atom site positions is that of Fig. 10.

recoil trajectories consist of predominately surface recoils³⁹ rather than direct recoils. These surface recoils are very sensitive to the underlying N interatomic spacings, which are short along the 0° and 60° directions where deep minima are observed and long along the 30° and 90° directions where maxima are observed. Combining the results from the two domains provides a symmetrical δ scan which is in good agreement with the experimental δ scan, with the exception of the small minima at the 30° and 90° azimuths. This latter discrepancy is due to blocking of H atom trajectories by neighboring H (self-blocking) and N atoms and is very sen-

Autocompensated $\text{GaN}\{000\bar{1}\}$ -(1x1)

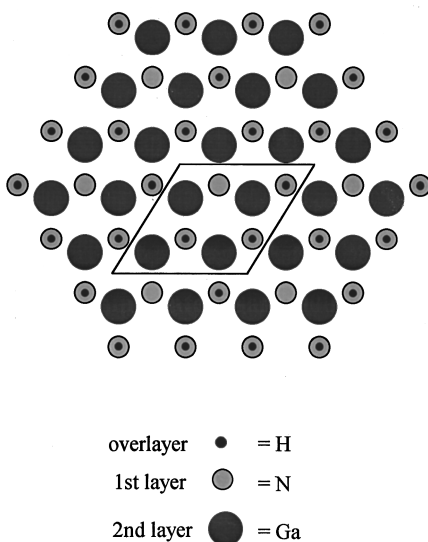


FIG. 10. Plan view of the ideal bulk-terminated $\text{GaN}\{000\bar{1}\}$ surface illustrating the surface (1×1) unit cell and a proposed model for the surface H atom sites. Open circles, first-layer N atoms; large solid circles, second-layer Ga atoms; small solid circles, overlayer H atoms. The sizes of the circles are proportional to the atomic radii.

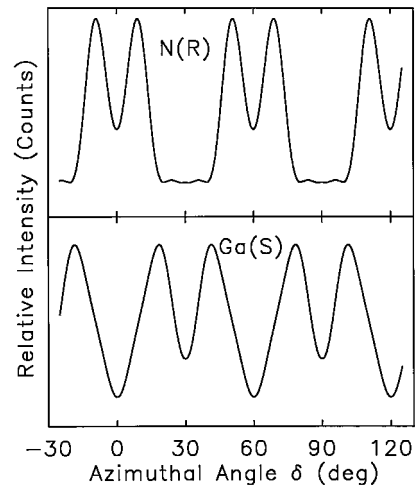


FIG. 11. Trajectory simulations of the azimuthal angle δ scans for N atoms recoiling from Ar^+ projectiles and Ar^+ projectiles scattering from Ga atoms for a Ga-terminated $\text{GaN}\{000\bar{1}\}$ -(1x1) surface, i.e., the first layer is composed of Ga atoms and the second layer is composed of N atoms.

sitive to the screening factor of the potential function which has not been established for H atoms. Nevertheless, the simulation using the $\frac{3}{4}$ monolayer model of Fig. 10 provides a better fit to the experimental scan than a model with a full monolayer coverage as shown in Fig. 6.

3. Simulations of the azimuthal scans of the Ga-terminated $\text{GaN}\{000\bar{1}\}$ -(1x1) surface

Simulations similar to those of Figs. 7–9 were carried out for a $\text{GaN}\{000\bar{1}\}$ -(1x1) surface in which the Ga and N atoms are exchanged, i.e., the first layer is composed of Ga atoms and the second layer is composed of N atoms. The results, presented in Fig. 11, show that the simulated data are in poor agreement with the experimental data. For N recoil, the $\{000\bar{1}\}$ simulation exhibits the deep minima at $\delta=30^\circ$ and 90° ; the $\{000\bar{1}\}$ simulation (Fig. 7) exhibits the deep minima at 0° and 60° , in agreement with the experimental data of Fig. 6. For scattering from Ga, the $\{000\bar{1}\}$ simulation exhibits the deep minima at $\delta=0^\circ$ and 60° ; the $\{000\bar{1}\}$ simulation (Fig. 8) exhibits the deep minima at 30° and 90° , in agreement with the experimental data of Fig. 6. These simulations show that termination of the surface as $\{000\bar{1}\}$ with Ga in the outermost layer is inconsistent with the δ scans.

D. Thermal decomposition of GaN

The LEED pattern, TOF-SARS spectra, and MS of the residual gases were monitored every 50°C while heating a GaN crystal. Beginning at low temperature with an uncleaned sample, the LEED image was completely diffuse and the TOF-SARS spectrum was dominated by H, C, O, and N recoil peaks. At a temperature of $\sim 700^\circ\text{C}$, the recoil impurities in the TOF-SARS spectrum began to decrease until the spectrum was eventually similar to that of Fig. 2. The diffuse LEED image evolved into a (1×1) pattern at $\sim 800^\circ\text{C}$; also at this temperature the MS exhibited sharp increases in the N_2^+ , NH_2^+ , and H_2^+ signals. The absence of an NH^+ signal may be due to its relative instability and the absence of direct

line of sight between the sample surface and the MS. The N_2^+ and NH_2^+ signals increased by a factor of $\sim 10^2$ between 800 °C and 900 °C, after which their intensities reached a plateau level which persisted to about 1050 °C. The H_2^+ signal increased monotonically by a factor of ~ 10 over this temperature range. The large amount of hydrogen evolved indicates that the hydrogen is not only on the surface but also contained in the bulk crystal. The (1×1) LEED pattern began to get increasingly more diffuse and the N and H recoil peaks in the TOF-SARS spectrum decreased as the temperature increased above 950 °C.

IV. DISCUSSION

A. Termination of $GaN\{000\bar{1}\}-(1 \times 1)$

Our results show that the $GaN\{000\bar{1}\}-(1 \times 1)$ surface is bulk terminated in a N layer with Ga comprising the second layer. The measured first-second-interlayer spacing agrees with the bulk spacing within the accuracy of the measurement, i.e., ± 0.2 Å. The nature of the termination layer is expected on the basis of polarity matching considerations between the substrate and film. Recent *ab initio* total energy calculations by Capaz *et al.*²⁸ have shown that the lowest-energy interfaces are expected to be those on which cations (anions) of the substrate bind to anions (cations) of the film. Hence, the final polarity of the film is strongly dependent on the initial stages of the growth process. The $\{0001\}$ sapphire substrate is oxygen terminated, therefore initial film growth in the form of Ga atoms bonding to O atoms is favored on clean sapphire. However, the low-temperature nucleation layer is grown by initial exposure of sapphire to NH_3 . This most likely forms a AlN nucleation layer on which initial film growth in the form of Ga atoms bonding to N atoms is favored. The packing sequence of the GaN wurtzite structure is $(\cdots ABAB \cdots)$, where the layers are not equally spaced; the vertical spacing along the hexagonal $\langle 0001 \rangle$ direction is 0.63 Å within a bilayer and 1.95 Å between bilayers. Since the simplest stable unit of GaN is a single bilayer consisting of a layer of Ga and N atoms, if growth commences with a Ga layer, it must terminate with a N layer. The only other experimental work known to us on identifying GaN polarity matching is for GaN grown on SiC by Sasaki and Matsuoka.¹⁵ This work addresses the problem indirectly by measuring the XPS chemical shift of the Ga atoms near the surface resulting from bonding to impurity oxygen atoms. Since the oxygen diffuses into the GaN to a depth of a few atomic layers and XPS samples a similar depth, the measurement is not specific to the outermost atomic layer. The conclusion¹⁵ was that GaN layers on $\{000\bar{1}\}_C$ and $\{0001\}_{Si}$ SiC substrates are terminated with Ga and N, respectively, in contradiction with the theoretical prediction²⁸ and our experimental results on GaN/Al_2O_3 .

B. Autocompensation and reconstruction

The bulk-terminated polar surfaces of compound semiconductor surfaces are typically unstable due to the partial electron occupancies of their dangling bonds.¹⁷ These surfaces achieve stability and semiconducting behavior by reconstructing in a manner in which the dangling bonds either

coalesce into dimer bonds or become completely filled or empty by electron transfer from the more electropositive to the more electronegative elements. Such a situation results in a semiconducting surface in which all dangling bonds are either completely filled or empty, i.e., it is autocompensated.^{37,40} A set of empirical autocompensation ‘‘principles’’ have been proposed¹⁷ which are based on a simple electron counting or ‘‘bookkeeping’’ description of the number of electrons in a system. These principles permit the prediction of chemically feasible structures and provide an understanding of why certain structures are unstable, subject to the constraints imposed by solid state effects. Although the principles are incapable of predicting which structure has the lowest energy, they are capable of interpreting¹⁷ the structures of all known semiconductor surfaces. We will apply these autocompensation concepts to interpretation of the results reported herein.

Consider a clean unreconstructed N-terminated $GaN\{000\bar{1}\}-(1 \times 1)$ surface. All N and Ga atoms are sp^3 hybridized, each second-layer Ga atom contributes $\frac{3}{4}e$ to each of its four bonds to neighboring N atoms, and each first-layer N atom contributes $\frac{5}{4}e$ to each of its three bonds to neighboring Ga atoms and to its dangling bond protruding from the surface. This results in N dangling bonds which each have $\frac{5}{4}e$ and, therefore, a deficiency of $\frac{3}{4}e$. Autocompensation of this surface can be achieved either by reconstruction or by bonding of these N dangling bonds to foreign atoms which can donate electron density to fulfill the deficiency; H atoms can fulfill this requirement. Since the surface is not reconstructed and H coverage of the N atoms was observed by TOF-SARS under all conditions where a (1×1) LEED pattern was observed, we propose that the surface is H stabilized. The N dangling bonds each require only $\frac{3}{4}e$ and each H atom contributes $1e$. Therefore, in order for the surface to be autocompensated, only $\frac{3}{4}$ of the outerlayer N atoms can be bound to H atoms. Considering the surface structure shown in Fig. 10, there are four N atoms in a unit cell. With three of these N atoms forming N-H bonds, there is a total excess of $\frac{3}{4}e$ from the three H atoms which can be transferred to the fourth N atom in order to fill its dangling bond. This results in a H atom coverage of $\frac{3}{4}$ of a monolayer; $\frac{3}{4}$ of the N dangling bonds are bonded to H atoms and the remaining $\frac{1}{4}$ are each filled with $2e$. There are several patterns in which these H atoms can be distributed on a N-terminated GaN surface; the model of Fig. 10 represents only one of these possibilities. This particular model was chosen because its simulated δ scan [Fig. 9, curve $(D_1 + D_2)$] provides better agreement with the experimental δ -scan (Fig. 9, expt.) than any of the other models used. For a surface covered with an ordered $\frac{3}{4}$ monolayer of an adsorbate, one might expect to observe higher order diffraction rods. This was not observed, possibly because H is a weak scatterer, there may be different models and mixed domains of the H atom patterns, and there may be considerable disorder in the H adlayer.

Some research groups²² using MBE growth, where hydrogen is either totally absent or in negligible concentration, have observed streaky (2×2) RHEED patterns. Such a (2×2) reconstruction could be in the form of a $GaN\{000\bar{1}\}-p(2 \times 2)$ -N vacancy, similar to that for Ga-rich surfaces proposed for the $GaAs\{111\}-p(2 \times 2)$ structure.¹⁷ Such a reconstruction can stabilize the surface in the absence of foreign

atoms, such as H, for termination of the dangling bonds. *Our results suggest that an important factor in the growth of high crystalline quality GaN is the presence of hydrogen to stabilize the dangling bonds of the evolving crystal surface.* Termination of the surface by H atoms during growth maintains sp^3 hybridization of the evolving Ga and N layers, resulting in less ionic character.

C. Hydrogen in GaN growth

There is plenty of hydrogen available in OMVPE growth to fulfill the monolayer coverage requirement. In the case of MBE growth, it has been shown^{21,41} that the use of ammonia rather than nitrogen as a source gas results in higher crystalline quality GaN. The relative ease of dissociation of NH_3 compared to N_2 has been used to explain²¹ this result. Of the possible sources of hydrogen which can incorporate into the GaN film during OMVPE growth, H from decomposition of NH_3 is the most likely candidate. The N-H bond energy is $\sim 4.0\text{--}4.8$ eV.^{42,43} This is qualitatively observed in the initial temperature for H_2 desorption at 800 °C, which suggests an activation energy for H_2 desorption of 2.9–3.5 eV.⁴⁴ NH_3 decomposition to form H_2 and N_2 should become significant at temperatures as low as 500 °C;⁴⁵ however, there is likely a substantial barrier to NH_3 gas phase decomposition. Large amounts of NH_3 compared to $Ga(CH_3)_3$ (the V/III ratio is typically >1000) are necessary for OMVPE growth of stoichiometric GaN films.³ There are two possible reasons for this. First, complete decomposition of the NH_3 to H_2 and N_2 inactivates the nitrogen for GaN growth. Second, at the OMVPE growth pressure (57 torr) and temperature (1040 °C) used, there may be enhanced “annealing” due to dynamic adsorption and desorption of Ga and N. Recent recoil ion mass spectroscopy studies showed that a D-terminated polycrystalline GaN surface could be converted to a H-terminated surface using NH_3 at room temperature.⁴⁶ This study suggests that the surface may assist in breaking the first N-H bond, allowing the NH_3 to adsorb onto the surface. Clearly, the breaking of the last N-H bond, whether in the gas phase or on the surface, is potentially a rate limiting step for N incorporation into the GaN lattice. This is precisely what is observed in films cooled in an NH_3 flux. If the H is attached to the N, then this is potentially the last N-H bond to be broken—the surface N-H bond.

D. Hydrogen in GaN

Two of the experimental results concerning hydrogen are especially noteworthy. First, it was not possible to eliminate hydrogen from the GaN surface in the TOF-SARS chamber, even after cycles of N_2^+ sputtering and annealing. This result is unprecedented in our work. In previous studies on semiconductor [Si,⁴⁷ Ge,⁴⁸ GaAs,³⁵ InAs,³⁵ GaP,⁴⁹ and InP (Ref. 37)] and metal [W,^{36,38} Ni,⁵⁰ Pt,⁵¹ and Ir (Ref. 52)] surfaces, it was always possible to clean the surfaces to a level where the hydrogen was below the TOF-SARS detection limit ($<10^{13}$ H atoms/cm²). This inability to eliminate hydrogen from the GaN surface implies that it is being replenished as rapidly as it is sputtered or desorbed off the surface. At the partial pressure of H_2 in our chamber, it would take $\sim 10^4$ sec

to have a monolayer of hydrogen contamination, assuming unit sticking probability. Also, there are no hot filaments in direct line of sight with the sample surface. Our results show that the concentration of hydrogen in the region from the surface down to some 1 000 nm (4.0×10^{19} atoms/cm³) is low, but sufficient to provide a reservoir for maintaining the observed surface monolayer hydrogen coverage (1.5×10^{16} atoms/cm²). Second, the H_2 and NH_2 species are evolved coincident with the evolution of N_2 resulting from thermal decomposition of GaN. This indicates that hydrogen in GaN is bound in the lattice as tightly as the Ga and N atoms themselves. For the reaction $GaN \rightarrow Ga + N_2$, $\Delta H = 1.15$ eV. A recent theoretical study⁹ has shown that H_2 in GaN is unstable towards dissociation into monatomic H. GaN is different from other group III-V compounds in that it has significant ionic character; the highly polarized GaN bonds provide regions of high electron density near the N atoms. The bond strength, position, and diffusivity of the hydrogen depends on its charge state.⁹ It is predicted that positively charged H^+ atoms prefer sites near the N atoms where they can be effectively screened, the H-N bond length is similar to that of NH_3 , and the migration barrier is 0.7 eV, i.e., sufficiently small for high mobility even at moderate temperatures. Negatively charged H^- is predicted to reside at tetrahedral interstitial sites and has a large migration barrier of ~ 3.4 eV, thus a very limited mobility. Neutral hydrogen H^0 is found to have only small energy differences between the various sites. Since our results were obtained on *n*-type GaN, they are consistent with the low solubility and diffusivity of H^- .

Hydrogen termination of the GaN surface may explain the apparent lack of surface states,³¹ i.e., these states are compensated, similar to the lack of surface states on H-terminated diamond surfaces. A recent O_2 chemisorption study³¹ has confirmed that GaN appears to have surface electronic states near the band edges or that they might lie higher up in the conduction band and therefore not observable in the band gap.

V. CONCLUSIONS

The most significant results on GaN{000 $\bar{1}$ }-(1×1) derived from the LEED, TOF-SARS, MS, ERD, and simulation data can be summarized as follows.

(i) The experimental and simulated azimuthal scans show that the (1×1) surface is bulk terminated with no detectable reconstruction or relaxation within the uncertainty of the measurement, i.e., ± 0.2 Å.

(ii) The surface elemental analysis, ASEA values, and experimental and simulated azimuthal scans consistently show the following: (a) the surface is terminated in a \bar{N} layer with Ga comprising the second layer, i.e., the {000 $\bar{1}$ } plane. (b) Hydrogen atoms are bound to the outermost N atoms with a coverage of $\sim \frac{3}{4}$ monolayer and protrude outward from the surface.

(iii) Thermal decomposition of the structure commences at ~ 850 °C with the evolution of N_2 , NH_2 , and H_2 . The presence of NH_x species provides strong evidence for N-H bonds on the surface. The high temperature required for evolution of the hydrogen indicates that it is as strongly bound as the Ga and N lattice atoms.

(iv) The large amount of H₂ evolved is consistent with hydrogen being distributed in the bulk of the crystals as well as on its surface. The ERD measurement yields a uniform concentration at a level of $\sim 4 \times 10^{19}$ H atoms/cm³ below the surface down to the sampling depth of ~ 1 000 nm.

(v) The azimuthal and incident angle scans are consistent with the existence of two structural domains on the surface which are rotated by 60° from each other and the incident angle scans indicate the presence of a significant amount of steps on the surface.

ACKNOWLEDGMENTS

This material is based on work supported by the National Science Foundation under Grant No. CHE-9321899 and the R. A. Welch Foundation under Grant No. E656. We thank Z. Zhang and W. K. Chu of the Texas Center for Superconductivity for ERD analysis of the GaN. We also graciously thank Vic Bermudez for initiating the collaboration between the NRL and UH groups and for numerous discussions on the GaN surface structure.

*Author to whom correspondence should be sent.

- ¹R. F. Davis, Proc. IEEE **79**, 702 (1991).
- ²S. Strite and H. Morkoc, J. Vac. Sci. Technol. B **10**, 1237 (1992).
- ³S. N. Mohammad, A. A. Salvador, and H. Morkoc, Proc. IEEE **83**, 1306 (1995).
- ⁴J. E. Jaffe, R. Pandey, and P. Zapol, Phys. Rev. B **53**, 4209 (1996).
- ⁵S. Nakamura, M. Senoh, and T. Mukai, Appl. Phys. Lett. **64**, 1687 (1994).
- ⁶H. Morkoc and S. N. Mohammad, Science **267**, 51 (1995).
- ⁷S. Nakamura, M. Senoh, S. Nagahama, N. Iwasa, T. Yamada, T. Matsushita, H. Kiyoku, and Y. Sugimoto, Jpn. J. Appl. Phys. **35** L74 (1996).
- ⁸D. K. Gaskill, A. E. Wickenden, K. Doverspike, B. Tadayon, and L. B. Rowland, J. Electron. Mater. **24**, 1525 (1995).
- ⁹J. Neugebauer and C. G. Van de Walle, Phys. Rev. Lett. **75**, 4452 (1995).
- ¹⁰R. G. Wilson, S. J. Pearton, C. R. Abernathy, and J. M. Zavada, J. Vac. Sci. Technol. A **123**, 719 (1995).
- ¹¹S. Nakamura, N. Iwasa, M. Senoh, and T. Mukai, Jpn. J. Appl. Phys. **31**, 1258 (1992).
- ¹²H. Amano, M. Kito, K. Hiramatsu, and I. Akasaki, Jpn. J. Appl. Phys. **38**, L2112 (1989).
- ¹³J. Neugebauer and C. G. van de Walle, Appl. Phys. Lett. **68**, 1829 (1996).
- ¹⁴A. E. Wickenden and K. Doverspike (unpublished). SIMS showed an O concentration of 3×10^{17} cm⁻³ and a C concentration of 2×10^{16} cm⁻³.
- ¹⁵T. Sasaki and T. Matsuoka, J. Appl. Phys. **64**, 4531 (1988).
- ¹⁶For example, the *c*-axis lattice constant for GaN grown on sapphire was 0.03% smaller than for bulk GaN; see M. Leszczyński, T. Suski, H. Teisseyre, P. Perlin, I. Grzegory, J. Jun, S. Porowski, and T. D. Moustakas, J. Appl. Phys. **76**, 4909 (1994).
- ¹⁷For a recent review, see C. B. Duke, Scanning Microsc. **8**, 753 (1994).
- ¹⁸P. Boguslawski, E. L. Briggs, and J. Bernholc, Phys. Rev. B **51**, 17 255 (1995).
- ¹⁹V. M. Bermudez, R. Kaplan, M. A. Khan, and J. N. Kuznia, Phys. Rev. B **48**, 2436 (1993).
- ²⁰M. Asif Khan, J. N. Kuznia, D. T. Olson, and R. Kaplan, J. Appl. Phys. **73**, 3108 (1993).
- ²¹Z. Yang, L. K. Li, and W. I. Wang, Appl. Phys. Lett. **67**, 1686 (1995).
- ²²K. Iwata, H. Asahi, S. J. Yu, K. Asami, H. Fujita, M. Fushida, and S. Gonda, Jpn. J. Appl. Phys. **35**, L289 (1996) (GaN 2×2 patterns were observed for growth on sapphire from ECR-MBE); M. E. Lin, S. Strite, A. Agarwal, A. Salvador, G. L. Zhou, N. Teraguchi, A. Rockett, and H. Morkoc, Appl. Phys. Lett. **62**, 702 (1993); H. Liu, A. C. Frenkel, J. G. Kim, and R. M. Park, J. Appl. Phys. **74**, 6124 (1993).
- ²³J. Hedman and H. Martensson, Phys. Scr. **22**, 176 (1980).
- ²⁴R. Carin, J. P. Deville, and J. Werckmann, Surf. Inter. Anal. **16**, 65 (1990).
- ²⁵D. Troost, H.-U. Baier, A. Berger, and W. Monch, Surf. Sci. **242**, 324 (1991).
- ²⁶L. A. DeLouise, J. Vac. Sci. Technol. A **10**, 1637 (1992).
- ²⁷X.-Y. Zhu, M. Wolf, T. Huett, and J. M. White, J. Chem. Phys. **97**, 5856 (1992).
- ²⁸R. B. Capaz, H. Lim, and J. D. Joannopoulos, Phys. Rev. B **51**, 17 755 (1995).
- ²⁹L. B. Rowland, K. Doverspike, A. Giordana, M. Fatemi, D. K. Gaskill, M. Skowroski, and J. A. Freitas, Jr., in *Silicon Carbide and Related Materials*, edited by M. G. Spencer, R. P. Devaty, J. A. Edmond, M. A. Khan, R. Kaplan, and M. Rahman (Bristol Institute of Physics, 1994), p. 429.
- ³⁰A. E. Wickenden, L. B. Rowland, K. Doverspike, D. K. Gaskill, J. A. Freitas, Jr., D. S. Simons, and P. H. Chi, J. Electron. Mater. **24**, 1547 (1995).
- ³¹V. M. Bermudez, J. Appl. Phys. (to be published).
- ³²J. W. Rabalais, Science **250**, 521 (1990); O. Grizzi, M. Shi, H. Bu, and J. W. Rabalais, Rev. Sci. Instrum. **61**, 740 (1990).
- ³³M. M. Sung, V. Bykov, A. Al-Bayati, C. Kim, S. S. Todorov, and J. W. Rabalais, Scanning Microscopy **9**, 321 (1995).
- ³⁴E. S. Parilis, L. M. Kishinevsky, N. Yu. Turaev, B. E. Baklitzky, F. F. Umarov, V. Kh. Verleger, S. L. Nizhnaya, and I. S. Bitensky, *Atomic Collisions on Solid Surfaces* (North-Holland, New York, 1993).
- ³⁵M. M. Sung, C. Kim, and J. W. Rabalais, Nucl. Instrum. Methods Phys. Res. (to be published).
- ³⁶O. Grizzi, M. Shi, H. Bu, and J. W. Rabalais, Phys. Rev. B **40**, 10 127 (1989).
- ³⁷M. M. Sung, C. Kim, H. Bu, D. S. Karpuzov, and J. W. Rabalais, Surf. Sci. **322**, 116 (1995).
- ³⁸M. Shi, O. Grizzi, H. Bu, J. W. Rabalais, R. R. Rye, and P. Nordlander, Phys. Rev. B **40**, 10 163 (1989).
- ³⁹J. W. Rabalais, CRC Crit. Rev. Solid State Mater. **14**, 319 (1988).
- ⁴⁰M. D. Pashley, Phys. Rev. B **40**, 10 481 (1989).
- ⁴¹N.-E. Lee, R. C. Powell, Y.-W. Kim, and J. E. Greene, J. Vac. Sci. Technol. A **13**, 2293 (1995).
- ⁴²J. E. Huheey, *Inorganic Chemistry*, 2nd ed. (Harper & Row, New York, 1978).
- ⁴³*CRC Handbook of Chemistry and Physics, 55th ed.* edited by R. C. Weast (CRC Press, Cleveland, 1974). The calculation is based on a simple first-order kinetic model with an assumed prefactor of 10¹³.
- ⁴⁴Calculation based on the calculated equilibrium constant (K_{eq})

- using the temperature dependence of ΔH and ΔS from Ref. 42.
- ⁴⁵ Must be catalyzed with Fe, i.e., the Born-Haber ammonia synthesis technique.
- ⁴⁶ C.-M. Chiang, S. M. Gates, A. Bensaoula, and J. A. Schultz, Chem. Phys. Lett. **246**, 275 (1995).
- ⁴⁷ Y. Wang, M. Shi, and J. W. Rabalais, Phys. Rev. B **48**, 1678 (1993).
- ⁴⁸ Y. Wang, H. Bu, T. E. Lytle, and J. W. Rabalais, Surf. Sci. **318**, 83 (1994).
- ⁴⁹ M. M. Sung and J. W. Rabalais, Surf. Sci. **365**, 136 (1996).
- ⁵⁰ H. Bu, C. Roux, and J. W. Rabalais, Surf. Sci. **271**, 68 (1992).
- ⁵¹ F. Mason and J. W. Rabalais, Surf. Sci. **253**, 245 (1991); **253**, 258 (1991).
- ⁵² H. Bu, M. Shi, and J. W. Rabalais, Surf. Sci. **236**, 135 (1990).